Multi-particle states of semiconductor hexagonal rings: Artificial benzene

Ana Ballester, Josep Planelles, and Andrea Bertoni

Citation: J. Appl. Phys. **112**, 104317 (2012); doi: 10.1063/1.4766444
View online: http://dx.doi.org/10.1063/1.4766444
View Table of Contents: http://jap.aip.org/resource/1/JAPIAU/v112/i10
Published by the American Institute of Physics.

Additional information on J. Appl. Phys.

Journal Homepage: http://jap.aip.org/
Journal Information: http://jap.aip.org/about/about_the_journal
Top downloads: http://jap.aip.org/features/most_downloaded
Information for Authors: http://jap.aip.org/authors

ADVERTISEMENT

Downloaded 07 May 2013 to 150.128.148.186. This article is copyrighted as indicated in the abstract. Reuse of AIP content is subject to the terms at: http://jap.aip.org/about/rights_and_permissions

Multi-particle states of semiconductor hexagonal rings: Artificial benzene

Ana Ballester,[1] Josep Planelles,[1] and Andrea Bertoni[2,a)]
[1]*Departament de Química Física i Analítica, Universitat Jaume I, P.O. Box 224, E-12080 Castelló, Spain*
[2]*Centro S3, CNR—Istituto Nanoscienze, Via Campi 213/A, 41125 Modena, Italy*

(Received 8 September 2012; accepted 20 October 2012; published online 20 November 2012)

We present a theoretical and numerical investigation of correlated multi-electron states of hexagonal semiconductor rings. Both single-particle and correlated states show localization patterns in the six corners and energy spectra degeneracies corresponding to a hexagonal benzene ring. Thus, our results can aid the interpretation of energy-loss or near-field experiments that, in turn, shed light on the nature of molecular few-particle orbitals of artificial benzene. Surprisingly, we find that charges get more localized in the corners as the number of electrons increases, up to six, this indicating the deficiency of a picture based on orbitals delocalized on the whole ring. We also expose the presence of several spin-correlated states and the effect of an asymmetry of the system. © *2012 American Institute of Physics*. [http://dx.doi.org/10.1063/1.4766444]

I. INTRODUCTION

Hexagonal shape is rather common in semiconductor nanowires (NWs) due to the crystal structure of the composing material.[1–4] Furthermore, a modulation in the NWs composition along the axis can lead to a further confinement of the free carriers and form a disk-shaped quantum dot whose effective two-dimensional (2D) potential results to be harmonic.[5] This essentially hides the real shape of the semiconductor pillar, i.e., the NW, from which the zero-dimensional confinement is obtained. Deep insight has been achieved on this type of nanostructures, including the nature of correlated few-particle states,[6,7] their relaxation rates,[8,9] and optical properties.[10,11]

Recently, a new kind of quasi-1D nanostructure, namely semiconductor core-multishell nanowires (CSNWs), has been realized,[12] where the carrier confinement is not limited to the center of the NW. This leads to additional degrees of freedom and interesting properties for applications in opto- and nano-electronic devices.[13]

In analogy with the fabrication of vertical or disk-shaped quantum dots from a NW, a proper material modulation along a CSNW axis should be able to generate a strong confinement of the carriers in that direction, leading to an effective 2D system. However, now the confinement in the orthogonal plane is not harmonic, and the shape of the CSNW section cannot be considered circular anymore. Rather, the carriers will be confined in a polygonal flat quantum ring. Our study addresses few-interacting-carrier states of semiconductor hexagonal rings. Due to the qualitative similarity of the system shape and symmetry with a benzene hexagonal ring, we term it *artificial benzene*. As we shall see, the few-electron density localization and the states degeneracies reflect the hexagonal symmetry as in benzene.

We focus on structures where electrons are localized on a square-well type potential in the radial direction, rather than being confined at the heterointerface by the triangular well generated by the band bending.[14,15] In fact, in the latter case, a large carrier density is needed in order to create a stable electron gas, thus concealing the correlation effects proper of the few-electron regime. We adopt an envelope function approximation for the single-particle wave functions and a full configuration interaction (FCI) approach to compute the correlated states. The FCI method provides both ground and excited states with comparable accuracy, this being essential in the calculation of electron-phonon interactions, response functions, and optical properties.[16,17]

This paper is organized as follows. In Sec. II, we describe the model of our physical system and in Sec. III, we outline the numerical approach adopted. In Sec. IV, the single-electron states are reported and in Sec. V, the correlated few-electron states are described with particular emphasis to their spin configuration and charge-density distribution. In Sec. VI, we address a system where the hexagonal symmetry is lifted by a thicker layer in one of the facets. Finally, in Sec. VII, we draw our conclusion.

II. THE PHYSICAL SYSTEM

The system we consider is constituted by a three-layer AlAs-GaAs-AlAs CSNWs with hexagonal cross section, where an additional strong confinement has been introduced in the growth direction. This gives an effective 2D system, where an hexagonal GaAs quantum well is wrapped around the AlAs core, as depicted in Figure 1. Since an excitation in the axial direction has an energy much larger than the energy scales involved in our simulations, we can neglect the motion in the (confined) axial direction and adopt an effective 2D model. To be specific, we consider a regular-hexagon domain with edges 66.5 nm long. The GaAs well is 6.8 nm wide. Its thickness is uniform all around the 37.3 nm AlAs core. This symmetry will be lifted in Sec. VI, where different thicknesses of one of the edges will be considered. The GaAs well is covered by a 13.5 nm AlAs capping layer. The conduction-band offset between the two materials is 438 meV. We consider an effective mass m^* isotropic on the ring plane, with $m^* = 0.063\, m_e$ ($m^* = 0.15\, m_e$) in GaAs (AlAs), and a dielectric constant $\varepsilon = 12.9\, \varepsilon_0$ ($\varepsilon = 10\, \varepsilon_0$) in

a)Electronic mail: andrea.bertoni@nano.cnr.it.

 © 2012 American Institute of Physics

Downloaded 07 May 2013 to 150.128.148.186. This article is copyrighted as indicated in the abstract. Reuse of AIP content is subject to the terms at: http://jap.aip.org/about/rights_and_permissions

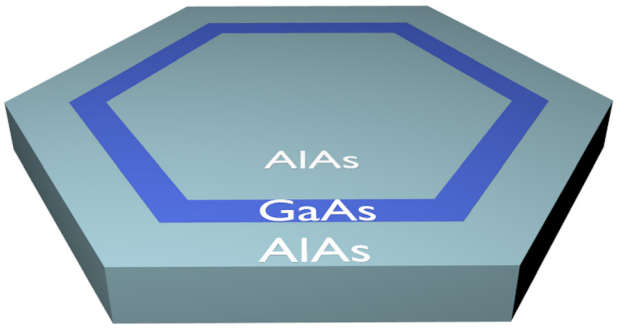

FIG. 1. Schematics of the system. A GaAs ring is wrapped around an hexagonal AlAs core and capped by an additional AlAs shell. The free electrons are confined in the GaAs region. A strong confinement in the axial direction leads to a ring-type structure.

GaAs (AlAs). An effective thickness $\tau = 2\,\text{nm}$ of the hexagonal ring in the axis direction is introduced in our model by means of an additional parameter that smooths Coulomb repulsion at short distance.[18,19]

III. NUMERICAL APPROACH

In order to find the correlated multi-electron states and assess the role of Coulomb interaction and correlation, we perform an exact diagonalization of the multi-particle Schrödinger equation via a FCI procedure. As a first step, the single-particle orbitals ψ_i and energies ϵ_i of a conduction-band electron are computed, for the confining structure described in Sec. II, through a numerical solution of the effective-mass Schrödinger equation

$$\left[-\frac{\hbar^2}{2}\nabla_{\mathbf{r}}\left(\frac{1}{m^*(\mathbf{r})}\nabla_{\mathbf{r}}\right)+E_c(\mathbf{r})\right]\psi_i(\mathbf{r})=\epsilon_i\psi_i(\mathbf{r}), \quad (1)$$

where $\mathbf{r}$ is the 2D coordinate on the hexagonal domain, $m^*(\mathbf{r})$ is the isotropic material-dependent effective mass of electrons, E_c is the conduction band profile, and i labels the single-particle state. The above equation is numerically integrated by means of a box integration method[20] on a triangular grid with hexagonal elements. The grid reproduces the symmetry of the system thus avoiding numerical artifacts originated by discretization asymmetries of the six domain boundaries, as would be the case, e.g., using a rectangular grid. Formally, the partial differential Eq. (1) is integrated on each hexagonal element. By applying the divergence theorem, the area integral is converted in a linear integral of the flux along the hexagon boundary. A balance between incoming and outgoing fluxes (obtained through a first-order finite-differences scheme) of adjacent hexagons connects the unknowns on different elements. This results in a symmetric sparse matrix whose dimension corresponds to the number of grid hexagons, and with seven non-zero elements on each row. This matrix is diagonalized through an efficient Lanczos library algorithm.[21] Our simulations typically use about 8600 hexagonal elements. Single-particle calculations are essentially irrelevant from the computational effort perspective. However, the discretization grid of the single-particle wave functions strongly affects the computational time of Coulomb integrals, as we detail in the following, and we had to choose a mesh thickness allowing for the practicable calculation of them, yet leading to a small numerical error (of the order of 1%) on the single-particle energies.

The next step is the calculation of the so-called Coulomb integrals

$$U_{ijkl}=\int d\mathbf{r}\int d\mathbf{r}'\,\psi_i^*(\mathbf{r})\psi_j^*(\mathbf{r}')\,\mathcal{U}(\mathbf{r}-\mathbf{r}')\,\psi_k(\mathbf{r}')\psi_l(\mathbf{r}), \quad (2)$$

which we perform by exploiting the hexagonal tessellation of the domain described above. In the equation above, $\mathcal{U}(\mathbf{r})=\frac{e}{4\pi\epsilon(\mathbf{r})(|\mathbf{r}|+\tau)}$ is the Coulomb potential energy between two electrons at distance $|\mathbf{r}|$. The cutoff parameter τ avoids divergences of the integrand: It mimics the effect of a finite thickness of the nanostructure in the axial direction as mentioned in Sec. II.

The multi-particle Hamiltonian matrix is then built up. First, we fix a number N of interacting electrons. Then, we build the Hilbert space by generating all possible Slater determinants $|\Phi_n\rangle$, that is, the multi-particle basis of the Hilbert space. For all the calculations presented in the following sections, we use 24 spin-orbital single-particle states, giving $\binom{24}{N}$ Slater determinants. In fact, we found that only the lowest 12 states, corresponding to the first 6 orbitals, are populated with a significant probability. We present calculations up to $N=7$, which need a basis of about 350×10^3 Slater determinants.

Finally, we compute the Hamiltonian matrix elements

$$H=\sum_{i\sigma}\varepsilon_i e_{i\sigma}^\dagger e_{i\sigma}+\frac{1}{2}\sum_{ijkl}\sum_{\sigma\sigma'}U_{ijkl}e_{i\sigma}^\dagger e_{j\sigma'}^\dagger e_{k\sigma'}e_{l\sigma}, \quad (3)$$

where $e_{i\sigma}$ ($e_{i\sigma}^\dagger$) is the annihilation (creation) operator for an electron in the orbital state i and with spin σ. The Hamiltonian matrix is finally diagonalized, leading to the complex coefficients C_n^m of the mth multi-particle state

$$|\Psi_m\rangle=\sum_n C_n^m|\Phi_n\rangle. \quad (4)$$

In order to obtain the real-space electron density of $|\Psi_m\rangle$, we compute

$$n(\mathbf{r})=\sum_{n_1,n_2}\left[(C_{n_1}^m)^*C_{n_2}^m\sum_\sigma\sum_{ij}\psi_i^*(\mathbf{r})\psi_j(\mathbf{r})\times\langle\Phi_{n_1}|e_{i\sigma}^\dagger e_{j\sigma}|\Phi_{n_2}\rangle\right], \quad (5)$$

while, for the conditional density, if an electron is found in $\bar{\mathbf{r}}$ with spin $\bar{\sigma}$, the density distribution of the remaining electrons with spin σ is

$$n(\mathbf{r},\sigma)|_{\bar{\mathbf{r}}\bar{\sigma}}=\sum_{n_1,n_2}\left[(C_{n_1}^m)^*C_{n_2}^m\sum_{ij}\sum_{kl}\psi_i^*(\mathbf{r})\psi_j^*(\bar{\mathbf{r}})\psi_k(\bar{\mathbf{r}})\psi_l(\mathbf{r})\times\langle\Phi_{n_1}|e_{i\sigma}^\dagger e_{j\bar{\sigma}}^\dagger e_{k\bar{\sigma}}e_{l\sigma}|\Phi_{n_2}\rangle\right]. \quad (6)$$

Downloaded 07 May 2013 to 150.128.148.186. This article is copyrighted as indicated in the abstract. Reuse of AIP content is subject to the terms at: http://jap.aip.org/about/rights_and_permissions

IV. SINGLE-ELECTRON STATES

The hexagonal symmetry of the GaAs quantum well gives a energy-level structure of the single-particle states with degeneracies 1-2-2-1, also typical of benzene molecule, as it is shown in Figure 2. In particular, we report in the figure, the colormaps of the lowest 12 wave functions with the corresponding energy reported on the right axis. The origin of the energy scale is set in the GaAs band gap, 60% of the gap below the bottom of the conduction band, where the Fermi level of the undoped structure should lie. As mentioned above, these single-particle states are obtained within the envelope function approximation.

In the FCI calculations reported in the following, we find that only the lowest 6 orbitals (spin-independent real-space wave functions) have significant population. Taking into account all 12 orbitals, we can identify two different types of shells, namely two groups of orbitals well separated in energy, having the same degeneracy pattern. They show different preferential localization of the wave functions. The first shell, ranging from 942.294 meV to 943.933 meV, contains the first 6 orbitals that accumulate the wave functions to the wider area around the hexagonal ring, i.e., at the corners. On the other hand, the second shell from 946.407 meV to 952.342 meV tends to localize the maxima of the wave functions along the edges of the hexagonal system, and consequently, has higher localization energy. Also, as expected, the number of nodes around the ring increases with increasing energy. In particular, we note that the double-degenerate first and second excited orbitals have one and two nodal lines, respectively. The following two orbitals have three nodal lines. However, they are not degenerate, being the last orbital of the first shell and the first one of the second shell. In fact, the electron density is modulated, so that six peaks are formed: in the first case, they are centered on the six corners, while in the second case, they are on the hexagon sides.

V. FEW-ELECTRON STATES

Multi-electron states are computed starting from the single-particle orbitals of Figure 2 by means of the FCI approach already described. Electron-density profiles up to $N = 7$ electrons reveal that Coulomb repulsion tends to localize electrons far from each other in order to minimize the electrostatic energy of the system, and the electron density for the lower-energy states accumulates on the corners of the hexagonal ring. This effect adds to the corner localization of single-particle states due to the wider area available and lower kinetic energy. In order to pick out the effect of the Coulomb interaction, in Figure 3, we report the electron density versus the position along an edge of the hexagon, for the multi-particle states up to seven electrons. The distribution is always higher at the corners, but the steepness decreases as the number of particles increases up to six, with the single-particle density higher in the middle of the edge than the six-particle one. In the latter case, the six electrons are highly localized on the six corners. This trend changes with the introduction of a seventh electron: since the lower kinetic-energy spots are all occupied the additional electron is

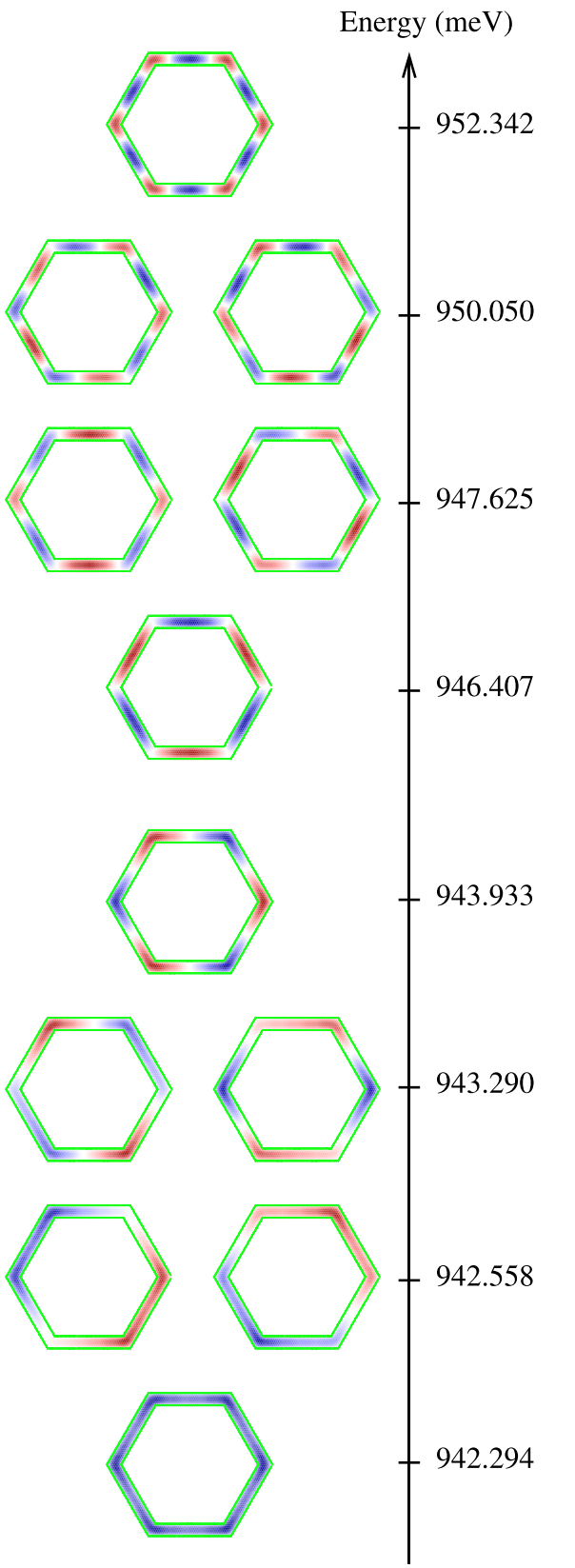

FIG. 2. Single-electron states $\Psi_i(\mathbf{r})$ for the hexagonal GaAs quantum well are represented, with red (blue) color indicating positive (negative) values. Due to the hexagonal symmetry, the electronic structure reproduces the benzene degeneracies distribution 1-2-2-1. We find two different wave function localization patterns depending on the energy: the first 6 states (first shell) stabilize their energy by accumulating the wave functions in peaks close to the corners of the hexagon, while the second 6 states (second shell) tend to localize the wave functions maxima along the edges.

Downloaded 07 May 2013 to 150.128.148.186. This article is copyrighted as indicated in the abstract. Reuse of AIP content is subject to the terms at: http://jap.aip.org/about/rights_and_permissions

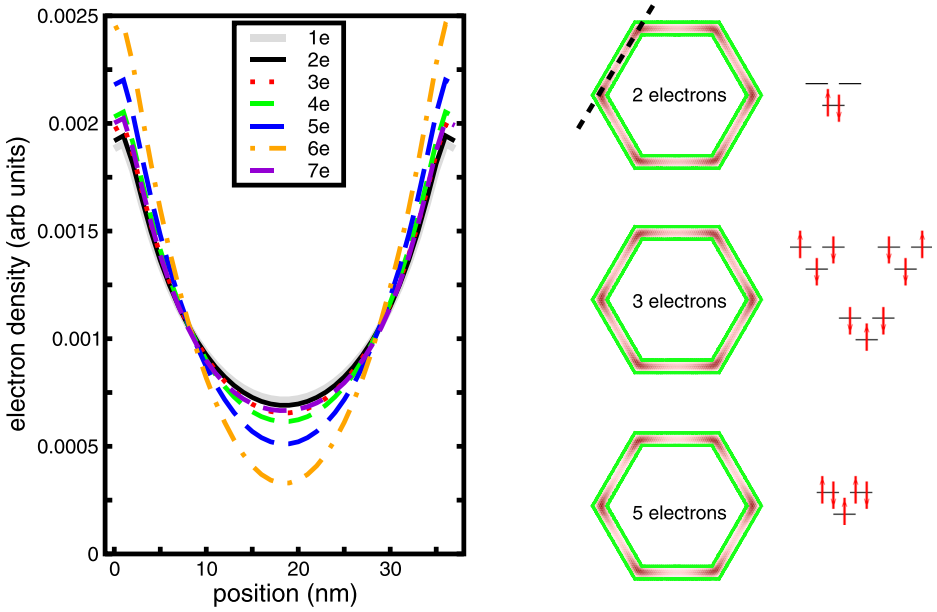

FIG. 3. Electron density along an edge (dashed line on the top right hexagon) for correlated ground states up to $N=7$. To ease the comparison, all the curves are normalized to unity. Most of the electron density is localized at the corners due to the Coulomb repulsion and lower kinetic energy. On the right, the colormap 2D plots for three cases are reported, together with their leading Slater determinants. Note that in the 3-electron case, the ground state is the spin-degenerate quadruplet $S=\frac{3}{2}$ and we plot here the state with $S_z=-\frac{1}{2}$, which has three leading Slater determinants entering the linear combination of Eq. (4) with the same coefficient.

delocalized on the whole ring. On the right part of Figure 3 we show, as an example, the electron density profiles of the ground multi-particle states with two, three, and five electrons, together with the schematic representation of the leading Slater determinant(s) $|\Phi_n\rangle$ in their configuration Eq. (4), i.e., the ones with largest $|C_n^m|^2$. To be specific, the short horizontal lines represent the three lower orbitals of Figure 2, and the arrows represent electrons with up or down spin.

Despite the similar density profiles, with high charge density on the six corners for all three cases, peculiar electronic configurations come into play in the correlated ground states. The 2-electron system attains a closed first shell as expected, while the 3-electron case shows an important contribution of electronic configurations, which do not follow the building-up and multiplicity principles, i.e., Aufbau's and Hund's rules, respectively.[22] An unusual leading configuration is also found for the 5-electron ground state, where electrons distribute in pairs in the two degenerate first-excited single-particle states forming a closed shell, while an unpaired electron lies in the first shell. However, we must stress that the above states are highly correlated, and in general, the higher the number of particles, the higher the effect of correlation. In fact, the weight of the leading Slater determinant for the two-particle state is 63%, while it is only 19% for the five-particle case.

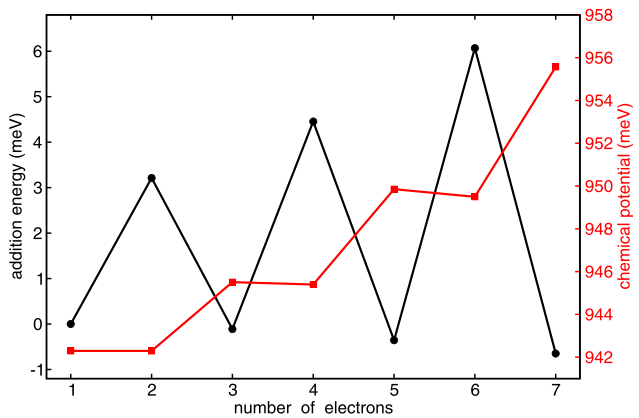

FIG. 4. Addition energies and chemical potential for different number of electrons. Two closed shells are formed at $N=2$ and $N=6$. A very stable configuration is also found for $N=4$, with the second shell half filled.

We also quantify the relative stability of the N-electron ground state by computing the addition energy, which is obtained using the formula

$$E_{add}(N) = E(N+1) - 2E(N) + E(N-1), \qquad (7)$$

where $E_{add}(N)$ is the energy required in order to place an extra electron into the system that has initially $N-1$ electrons. Such quantity, similar to electron affinity in atomic physics, is calculated by computing the total energy of the N-electron system ground state $E(N)$ and the total energies for the hexagon occupied with $N+1$ and $N-1$ electrons, i.e., $E(N+1)$ and $E(N-1)$, respectively.

The addition-energy spectrum is reported in Figure 4, together with the chemical potential, for different numbers of electrons. It reflects the orbital shell filling for the hexagonal symmetry up to $N=6$. The first shell is identified with the peak for 2 electrons, where system stabilizes because of the closed shell configuration. The degeneracy pattern of the symmetry of the system is observed when comparing 4- and 6-electron peaks. A half-filled shell is involved for the 4-electron configuration while a closed shell is formed for the 6-electron ground state. The extra stabilization effect for the closed shell can be detected thanks to the higher peak for six electrons. This six-electron case corresponds to that of a benzene ring. With seven electrons, the system stability decreases having a single unpaired electron in the two degenerate orbitals above two closed shells, resulting in a negative addition energy. The chemical potential versus the number of electrons is also reported on Figure 4.

In order to assess the effects of Coulomb-induced correlation on both ground state and excited states, we perform

Downloaded 07 May 2013 to 150.128.148.186. This article is copyrighted as indicated in the abstract. Reuse of AIP content is subject to the terms at: http://jap.aip.org/about/rights_and_permissions

conditional density calculations for several N-electron states and report the spatial distribution of the remaining $(N-1)$ electrons when one electron is found in a corner. In the 2-electron case, if an electron with spin up is fixed at one corner of the hexagon, spin down density is localized at the opposite corner as shown in Figure 5(a) for the 2-electron ground state. This Coulomb repulsion effect is also observed for excited states. For example, the double-degenerate second excited state is shown in Figure 5(b). Note that in order to preserve the symmetry of the system, a proper linear combination of the degenerate eigenstates resulting from the FCI procedure has to be considered. In fact, if a single correlated state is taken, its real-space density does not maintain the proper symmetry, as shown in Figure 5(c) and described in its caption. This is because we take Slater determinants as a basis and do not employ configuration state functions with the full system symmetry. In other words, we do not exploit quantum numbers originating from the hexagonal symmetry. This choice, although computationally expensive, gives us the freedom to alter the system geometry arbitrarily, as we will do in Sec. VI.

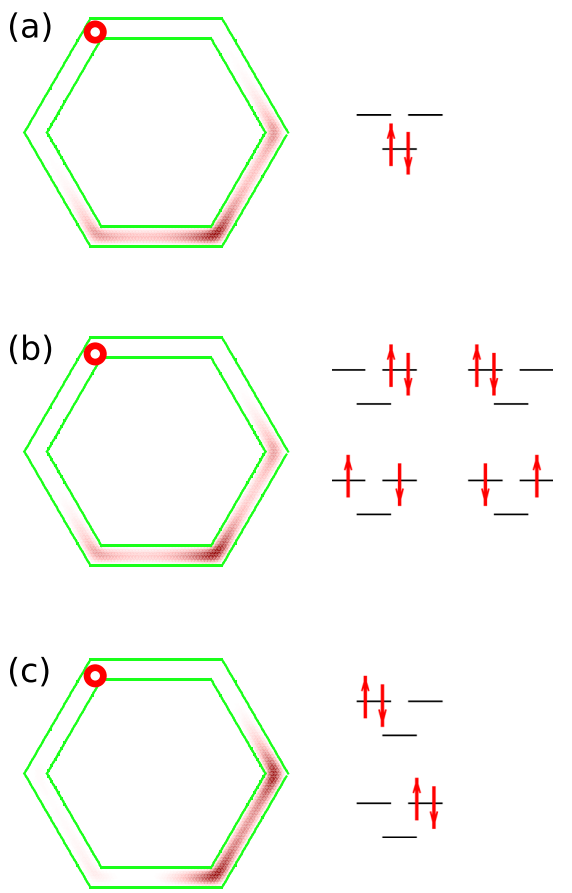

FIG. 5. Two electrons. Conditional densities, when one electron is fixed in one corner (small circle) for the ground state (a) and the double-degenerate second-excited state (b)-(c). While (b) shows the density of a proper linear combination of the two degenerate states yielding a correct symmetry, (c) shows the charge density of one of the states, as computed by our FCI approach. For each density plot, the leading Slater determinants composing the correlated state are reported on the right.

Next, we check the effect of electron-electron interaction on the correlation at higher electron densities. If we populate the hexagon with three electrons and we fix one of them in a corner, the other two are mainly found on the other two corners forming with the first one an equilateral triangle. This configuration is shown on the right of Figure 6, and it is the same for the four degenerate ground states forming the quadruplet with $S = \frac{3}{2}$. As already reported in Figure 3, this is a remarkable difference with respect to the non-correlated state, for which the ground state consists of two electrons in the lower orbital and one in the first-excited orbital, being this a $S = \frac{1}{2}$ state. The latter state will be also the ground one for the asymmetric system as we will show in Sec. VI. On the left part of Figure 6, we report the electron density along an edge, like in Figure 3. However, here, we fix the number of particles to three and report three different states. The more energetic the state, the more localized the electrons in the corners. Although the difference is small, we find that this effect is general, being present for any number of electrons, at least for the few lower states.

For the 4-electron case, we also address the spin density distribution. If one electron is fixed in a corner, the remaining particles are distributed along the rest of the system, with preferential localization in the opposite corner, as shown in Figure 7(a) for the 4-electron ground state. However, a remarkable difference is found between electrons with the same or opposite spin with respect to the fixed one. Let us fix an electron with spin down in a corner. While the other spin-down electron localizes as far as possible at the opposite corner of the hexagon, spin-up density is distributed at the next sides of the fixed electron, leaving the opposite corner empty. This is shown in Figure 7(b), on the right and left plots, respectively. This effect is much less effective in the excited states. In fact, the first excited state has a density distribution for same-spin electron (not shown) that resembles the one for ground state, i.e., in the opposite corner, while

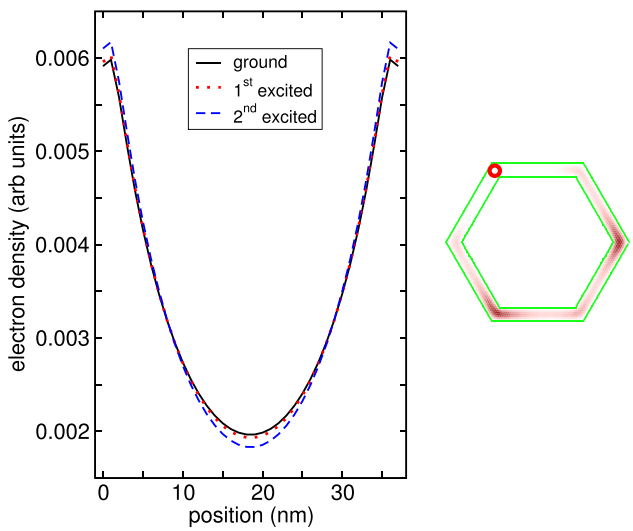

FIG. 6. Three electrons. Left: Density distribution along a hexagon edge for three different states. The higher the energy, the more localized the density in the corners. Right: Conditional density for the ground state when an electron is fixed in a corner. The other two electrons localize in two corners to form an equilateral triangle configuration.

Downloaded 07 May 2013 to 150.128.148.186. This article is copyrighted as indicated in the abstract. Reuse of AIP content is subject to the terms at: http://jap.aip.org/about/rights_and_permissions

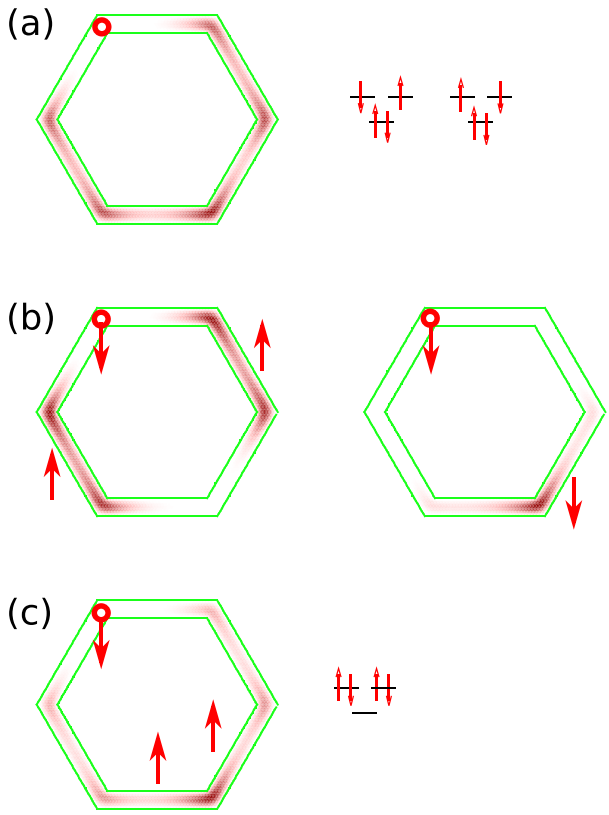

FIG. 7. Four electrons. (a) Conditional density for the ground state and its leading Slater determinants. (b) Ground-state conditional spin density for electrons with different (left) or same (right) spin as the fixed one. (c) Conditional spin density of the first-excited state (and its leading Slater determinant) for electrons with opposite spin with respect to the fixed one.

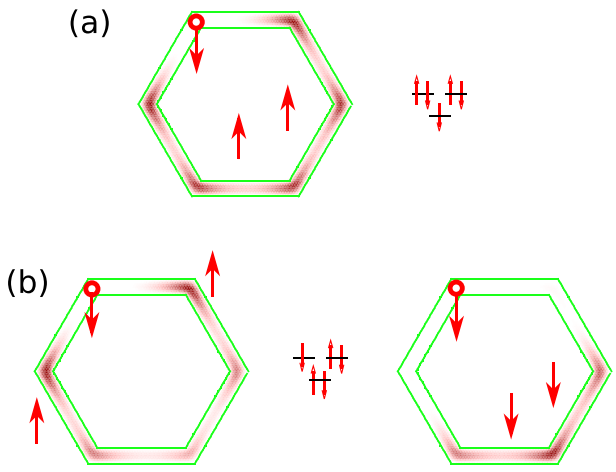

FIG. 8. Five electrons. (a) Conditional spin density for the ground state (and its leading Slater determinant) with spin opposite to that of the fixed particle. (b) Conditional spin density for the first excited state for both opposite-spin (left) and same-spin (right) cases. The leading Slater determinant of the first-excited state has lower energy than that of the ground state, this being an effect of Coulomb correlation. Spin distributions for the ground (first-excited) 5-electron case should be compared with the first-excited (ground) ones of the 4-electron case of Figure 7, where the shell-filling order is preserved.

opposite-spin electrons tend to localize at the opposite corner too, as shown in Figure 7(c).

Finally, the energy balance for a 5-electron system has a strong kinetic contribution. Electron density is high enough to distribute electrons all over the corners of the hexagon in the ground state, as shown in Figure 8(a) for the opposite-spin case (the same-spin case is similar). This is not true for the first excited state, where the density for the spin with the same orientation as the fixed particle is mainly localized at the opposite corner (Figure 8(b) on the right), while the opposite-spin density is distributed close to the fixed particle (Figure 8(b) on the left). It should be noted that here we find a ground state that does not follow Aufbau principle since in the leading Slater determinant, only one electron occupies the ground single-particle state. The correlated state corresponding to the non-interacting ground state is the first-excited one, shown in Figure 8(b). To assess the effect of larger electron number, the conditional spin distribution of Figure 8(b) should be compared with the ground 4-particle state in Figure 7(b). The behavior is qualitative similar, however in the 5-electron case, spin distributions are more spread, and for the opposite-spin case, the two spin-up peaks are in the two nearest-neighbor corners. This a Coulomb effect. In fact, the two remaining spin-down electrons are localized not only on the opposite corners but also spread across the other two corners as shown on the right of Figure 8(b).

VI. ASYMMETRIC HEXAGON

In this section, we analyze the case with one segment of the hexagonal ring thicker than the others. In fact, the experimental synthesis of semiconductor CSNWs achieved a very high control on the width of the overcoating semiconductor shells, as already described in the Introduction, with a nanometric precision. However, even a small deviation from the perfect symmetry of the six edges is expected to have a deep influence on the energy spectra and charge distributions of our hexagonal system. Therefore, we consider convenient to show the system's behavior when an asymmetry is introduced. Specifically, we take one edge of the hexagon up to 2 nm thicker than the others, while maintaining its inner border in the same position. We will refer to this kind of irregular system as an asymmetric hexagon.

At the single-particle level, the asymmetric spatial confinement is responsible for the breakdown of the degeneracies found in the symmetric case of Figure 2. The electron density of the lower states is now concentrated in the large edge and the energy of those states decreases dramatically. We report the energy spectrum of the first eight states as a function of the additional thickness of the hexagon top edge in Figure 9. As the thickness increases, more and more levels leave the energy of the symmetric case and decrease linearly. Moreover, levels from the upper shell (only two of them are shown in the graph) decrease as well, and join the lower shell. States with energy below that of the first shell of the symmetric system are mainly localized in the large edge. In fact, we focus on a specific case, with an extra top edge

Downloaded 07 May 2013 to 150.128.148.186. This article is copyrighted as indicated in the abstract. Reuse of AIP content is subject to the terms at: http://jap.aip.org/about/rights_and_permissions

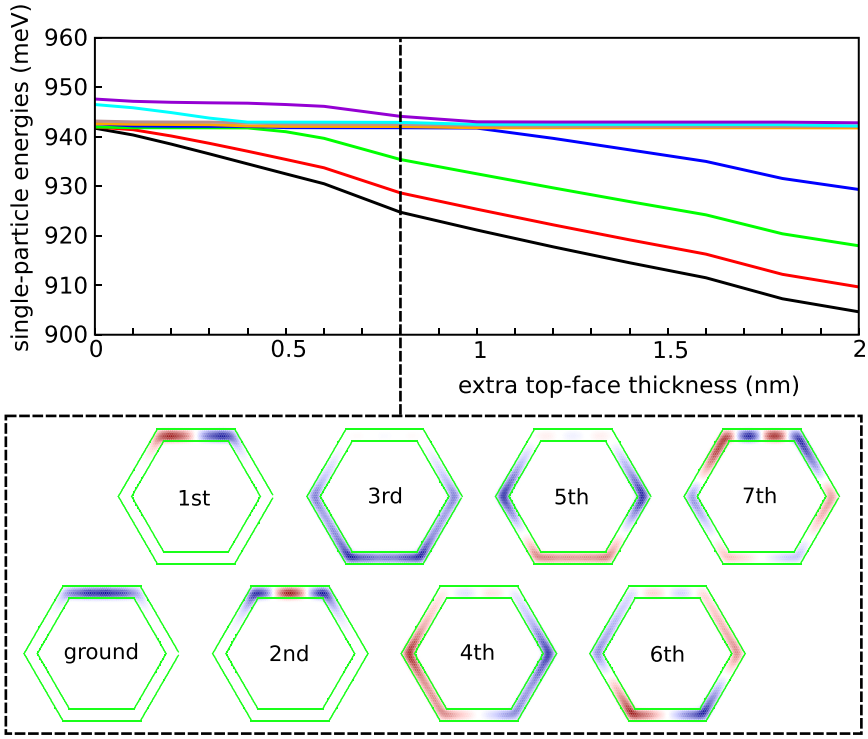

FIG. 9. Single-particle energies as a function of the additional thickness of the upper edge with respect to the symmetric hexagon. The lower panel shows several single-particle wave functions, in ascending energy order from left to right, for an extra thickness of 0.8 nm (dashed vertical line), i.e., with the larger edge 7.6 nm thick. Note that contrary to the multi-particle case, the part of the hexagon with a smaller thickness is occupied already from the third excited state.

thickness of 0.8 nm, i.e., 7.6 nm of total width, indicated by the dashed vertical line in Figure 9. The bottom panel shows the wave functions of such case, with increasing energy from left to right. Correspondingly, in the upper graph, we have three states with low (and linearly decreasing) energy. Indeed, the first three wave functions are localized in the top edge. The wave functions with higher energy have strong occupation in the rest of the hexagon and show an increasing number of nodal lines as in the symmetric case.

When including electron-electron interaction, the density profiles of the multi-electron states reflect the preferential localization in the top edge of the single-particle ones. However, Coulomb interaction tends to increase as much as possible the inter-particle distance. As a consequence, the density distribution is a balance between those effects, tailored by the number of electrons in the system. As an example, we show in the upper part of Figure 10, the charge density for three electrons (left) and seven electrons (right). In the first case, the particles are almost completely localized in the top edge, while in the second case, the larger electron density gives a high density also on the other four corners. In fact, with seven electrons, three of them are located in the top edge, and the remaining four are in the other corners, approximately. The effect of Coulomb correlation can be exposed by observing the conditional density for the 3-electron and 7-electron ground states (bottom graphs in Figure 10). While the conditional distribution for three electrons is what one would expect from a mean-field perspective, with the bottom part unchanged and a large density in the top edge around the opposite corner with respect to the fixed particle, the conditional density for seven electrons is fully located on the three opposite corners, in spite of the lower confining energy of the top ones.

Although the 3-electron conditional density resembles a mean-field solution, it results to be strongly spin-polarized, as shown in the top part of Figure 11. In fact, if we fix in a corner of the large edge a spin-down particle, we find that the charge localized on the other side of that edge has opposite spin, while the other spin-down electron is spread in the bottom edge and corners. We stress that the ground state is double spin-degenerate and that we are considering the state with $S_z = -\frac{1}{2}$. It means that a crossing between $S = \frac{3}{2}$ and

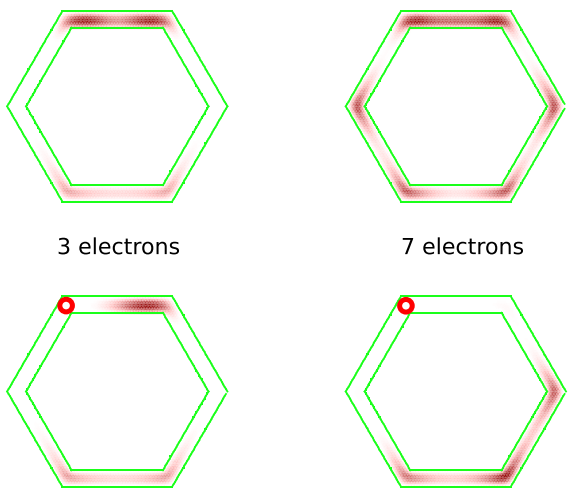

FIG. 10. Charge density (top) and conditional charge density (bottom) for the ground 3-electron (left) and 7-electron (right) state of the asymmetric hexagon described in Figure 9. In the lower-density case, the particles are completely localized in the large edge, while in the higher-density case, particles are also found in the other four corners. The conditional density distribution of the latter state shows nonlocal effects typical of strong correlation.

Downloaded 07 May 2013 to 150.128.148.186. This article is copyrighted as indicated in the abstract. Reuse of AIP content is subject to the terms at: http://jap.aip.org/about/rights_and_permissions

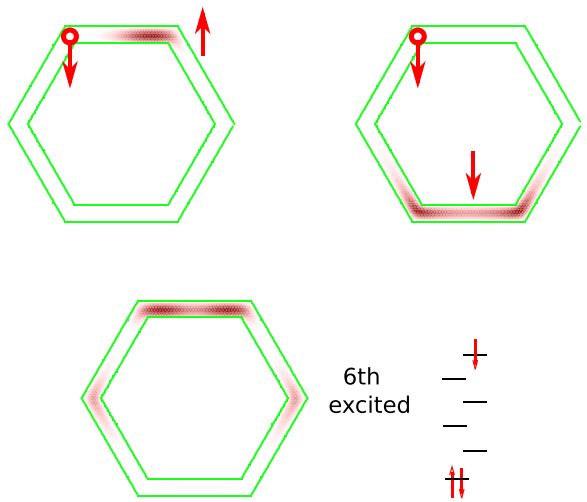

FIG. 11. Top: Conditional spin density for the ground 3-electron state of the asymmetric hexagon described in Figure 9. Two electrons with opposite spin form a two-particle state in the large edge while the other electron is completely localized in the two corners at the opposite edge. Bottom: The sixth excited state is the first one showing nonzero occupancy of the two lateral corners. The lower kinetic energy needed to occupy the larger edge also induces a preferential localization on the opposite edge and high energy is needed to occupy the remaining sites.

$S = \frac{1}{2}$ states occurs with the increase of the top edge thickness. In order to find some charge density in the two middle corners for the 3-electron case, we have to consider a high-energy state, namely the sixth excited, shown in Figure 11 together with its leading Slater determinant. This means that, while a system with higher electron density has all the corners occupied already in the ground state, a low-density asymmetric state not only localizes the charge mainly in the large edge, but completely removes electrons from the two middle corners.

VII. CONCLUSIONS

We have presented a numerical study of multi-electron states in hexagonal rings. We showed that the six corners are sites of preferential localization for electrons at both single-particle and correlated-particle levels. This makes our hexagonal system qualitatively similar to a benzene ring, where, according to its standard picture, six carbon atoms act as Coulomb centers, and six electrons are delocalized on a continuous π bond across the ring.[23] We find that in the artificial benzene system considered here, electron states are in general strongly correlated, and a picture of a single orbital delocalized on the whole ring is not appropriate.

We specifically considered an hexagonal quantum ring made by GaAs on an AlAs matrix, in analogy to CSNWs, but with an additional confinement along the axial direction. A number of ground and excited states have been addressed by analyzing their charge and spin density profiles. As the number of electrons populating the conduction band increases, stronger charge localization forms at the corners of the hexagon. However, the 7-electron ground state reveals that one electron is completely delocalized in the structure, above a closed, very stable, shell with one electron on each corner. As a consequence, the localization trend with electrons in the corners gets stronger up to six particles, then for seven particles, the density profile spreads substantially also along the edges. Although we do not find a general rule, we expose several specific ground and excited states with spin localization by considering opposite/same spin densities in conditional density calculations. We observe that opposite-spin densities tend to distribute as far as possible in order to minimize the energy of the system.

When the hexagonal symmetry is broken by the increase of an edge width, two effects are evident on the single-particle states: first, the 1-2-2-1 degeneracy pattern is broken, second, in low-energy states, the electron is mainly found in the large edge. On one hand, the above effects are not surprising, on the other hand, their consequences on the multi-particle states are of interest. For example, in the 3-electron case, we find a ground-state crossing between the symmetric ($S = \frac{3}{2}$) and the asymmetric ($S = \frac{1}{2}$) systems, while we find a highly correlated state for the 7-electron system, with consistent charge density on the corners opposite to the thick edge of the asymmetric system.

The understanding of correlation effects and the tailoring of charge localization patterns with the electron density, with asymmetries of the semiconductor structure or with external fields, are the first step towards an engineering of electronic and optical properties of semiconductor hexagonal rings. In fact, the study of artificial benzene, beside being of basic interest due to its analogy to a benzene ring, can expose the potentiality of such system for novel applications. Our methodology is the basis for both the calculation of intraband electronic and interband excitonic spectra. In fact, the calculation of multi-electron states alone can be useful to describe the far infra-red intraband spectra, but it cannot give hints on the optical properties of a nanosytem (related to interband near-UV and visible transitions). Exicton and multi-exciton spectra can be obtained once holes are also included in the calculations. However, in our paper, we focus on the multi-particle correlation in hexagonal geometry, and both the calculation of the far infra-red spectrum and the inclusion of holes are beyond the scope of our work and will possibly be a subject of future investigation.

Concerning the possible experimental fabrication of artificial benzene, we already mentioned in the Introduction how it could be obtained from a "slice" of a CSNW. In fact, while the length of CSNWs is only limited by their capability of sustaining themselves vertically while growing on a substrate and can reach several micrometers, their orthogonal shape depends on the crystallographic arrangements of their materials. In particular, most III-V NWs with a diameter less than about 400 nm grow as hexagonal crystals exposing the six 110 vertical facets normal to the (111) plane. For example, InAs/InAsP CSNWs grown on Si(111),[24] GaAs/AlAs CSNWs grown on GaAs(111)B,[2] and GaP/GaAs CSNWs grown on Si(111)[25] show a very neat hexagonal section in electron microscopy scans, even after a few overcoating processes. The overgrowth of different materials on the exposed facets leads to a prismatic heterostructure that confines eventually the free carriers either at the heterointerface or in the lower-gap semiconductor layer.[26] The two

Downloaded 07 May 2013 to 150.128.148.186. This article is copyrighted as indicated in the abstract. Reuse of AIP content is subject to the terms at: http://jap.aip.org/about/rights_and_permissions

confinement mechanisms are equivalent to that at the basis of planar two-dimensional electron gas (2DEG) formation in high-electron-mobility-transistors[27] and in rectangular quantum wells,[28] respectively. As a result, a 2DEG wrapped on the surface of an hexagonal prism can be formed.[29,33–36] The introduction of a strong confinement along the CSNW axis (e.g., via material modulation) would lead to a hexagonal ring.

Finally, we mention that the real-space electron distribution could be exposed though a near field spectroscopy. However, our hexagonal rings should lie on a substrate rather than being embedded in a CSNW in order to use such probing technique. In fact, experiments and simulations on Cu hexagonal vacancy islands clearly showed standing-wave patterns reflecting the hexagonal geometry.[30–32] Although the latter works could not reveal correlation effects due to the metallic nature of the nanometric system addressed, they demonstrated that spin polarization can be experimentally manipulated. A similar approach could be able to tailor few-particle spin-polarized states in hexagonal quantum rings.

ACKNOWLEDGMENTS

The authors thank Guido Goldoni, José Movilla, and Miquel Royo for valuable help. This work was partially supported by UJI-Bancaixa Project No. P1-1B2011-01, MCINN Project No. CTQ2011-27324, and FPI Grant (A.B.). EU Project INDEX (PITN-GA-2011-289968) is also acknowledged. Computing resources have been provided through CINECA ISCRA Project HP10CLLJ6S.

[1]F. Glas, J. C. Harmand, and G. Patriarche, Phys. Rev. Lett. **99**, 146101 (2007).
[2]A. Fontcuberta i Morral, D. Spirkoska, J. Arbiol, M. Heigoldt, J. R. Morante, and G. Abstreiter, Small **4**, 899 (2008).
[3]R. E. Algra, M. Hocevar, M. A. Verheijen, I. Zardo, G. G. W. Immink, W. J. P. van Enckevort, G. Abstreiter, L. P. Kouwenhoven, E. Vlieg, and E. P. A. M. Bakkers, Nano Lett. **11**, 1690 (2011).
[4]S. Hertenberger, S. Funk, K. Vizbaras, A. Yadav, D. Rudolph, J. Becker, S. Bolte, M. Doblinger, M. Bichler, G. Scarpa, P. Lugli, I. Zardo, J. J. Finley, M.-C. Amann, G. Abstreiter, and G. Koblmuller, Appl. Phys. Lett. **101**, 043116 (2012).
[5]L. Jacak, P. Hawrylak, and A. Wójs, *Quantum Dots* (Springer, 1998).
[6]C. P. García, V. Pellegrini, A. Pinczuk, M. Rontani, G. Goldoni, E. Molinari, B. S. Dennis, L. N. Pfeiffer, and K. W. West, Phys. Rev. Lett. **95**, 266806 (2005).
[7]J. Planelles, M. Royo, A. Ballester, and M. Pi, Phys. Rev. B **80**, 045324 (2009).
[8]J. I. Climente, A. Bertoni, G. Goldoni, and E. Molinari, Phys. Rev. B **74**, 035313 (2006).
[9]S. Amasha, K. MacLean, I. P. Radu, D. M. Zumbühl, M. A. Kastner, M. P. Hanson, and A. C. Gossard, Phys. Rev. Lett. **100**, 046803 (2008).
[10]S. Kalliakos, C. P. García, V. Pellegrini, M. Zamfirescu, L. Cavigli, M. Gurioli, A. Vinattieri, A. Pinczuk, B. S. Dennis, L. N. Pfeiffer, and K. W. West, Appl. Phys. Lett. **90**, 181902 (2007).
[11]J. I. Climente, A. Bertoni, and G. Goldoni, Phys. Rev. B **78**, 155316 (2008).
[12]G. Shen and D. Chen, Sci. Adv. Mater. **1**, 213 (2009).
[13]C. Colombo, M. Hei, M. Grätzel, and A. Fontcuberta i Morral, Appl. Phys. Lett. **94**, 173108 (2009).
[14]A. Bertoni, M. Royo, F. Mahawish, and G. Goldoni, Phys. Rev. B **84**, 205323 (2011).
[15]B. M. Wong, F. Lonard, Q. Li, and G. T. Wang, Nano Lett. **11**, 3074 (2011).
[16]A. Bertoni, M. Rontani, G. Goldoni, and E. Molinari, Phys. Rev. Lett. **95**, 066806 (2005).
[17]M. Rontani, C. Cavazzoni, D. Bellucci, and G. Goldoni, J. Chem. Phys. **124**, 124102 (2006).
[18]M. M. Fogler, Phys. Rev. Lett. **94**, 056405 (2005).
[19]W. Häusler and B. Kramer, Phys. Rev. B **47**, 16353 (1993).
[20]S. Selberherr, *Analysis and Simulation of Semiconductor Devices* (Springer, New York, 1984).
[21]R. B. Lehoucq, C. Sorensen, and D. C. Yang, *ARPACK Users Guide: Solution of Large-Scale Eigenvalue Problems with Implicitly Restarted Arnoldi Methods* (SIAM, Philadelphia, 1998).
[22]A. Franceschetti and A. Zunger, EPL **50**, 243 (2000).
[23]D. L. Cooper, J. Gerratt, and M. Raimondi, Nature **323**, 699 (1986).
[24]M. Keplinger, T. Martensson, J. Stangl, E. Wintersberger, B. Mandl, D. Kriegner, V. Holý, G. Bauer, K. Deppert, and L. Samuelson, Nano Lett. **9**, 1877 (2009).
[25]G. Zhang, K. Tateno, T. Sogawa, and H. Nakano, Appl. Phys. Express **1**, 064003 (2008).
[26]A. Nduwimana and X. Wang, Nano Lett. **9**, 283 (2009).
[27]S. M. Sze, *Modern Semiconductor Device Physics* (Wiley Interscience, 1998).
[28]T. Ando, A. B. Fowler, and F. Stern, Rev. Mod. Phys. **54**, 437 (1982).
[29]The analysis of a wrapped 2DEG with a cylindrical model simplifies the approach, in particular, if the effect of external magnetic fields is considered (Refs. 33 and 34), but in general, it is not adequate for prismatic CSNWs. In fact, it has been calculated that charge carriers tend to accumulate at the edges due to the wider area available for the carrier wave functions (Refs. 15 and 35) and, consequently, lower localization energy. This effect has been clearly demonstrated experimentally in the formation of so-called V-groove NWs (Ref. 36).
[30]L. Niebergall, G. Rodary, H. F. Ding, D. Sander, V. S. Stepanyuk, P. Bruno, and J. Kirschner, Phys. Rev. B **74**, 195436 (2006).
[31]O. O. Brovko, W. Hergert, and V. S. Stepanyuk, Phys. Rev. B **79**, 205426 (2009).
[32]A. S. Smirnov, N. N. Negulyaev, L. Niebergall, W. Hergert, A. M. Saletsky, and V. S. Stepanyuk, Phys. Rev. B **78**, 041405 (2008).
[33]G. Ferrari, A. Bertoni, G. Goldoni, and E. Molinari, Phys. Rev B **78**, 115326 (2008).
[34]V. Harutyunyan, G. Demirjian, and N. Gasparyan, Physica E **43**, 614 (2010).
[35]G. Ferrari, G. Goldoni, A. Bertoni, G. Cuoghi, and E. Molinari, Nano Lett. **9**, 1631 (2009).
[36]D. Kaufman, Y. Berk, B. Dwir, A. Rudra, A. Palevski, and E. Kapon, Phys. Rev. B **59**, R10433 (1999).

Downloaded 07 May 2013 to 150.128.148.186. This article is copyrighted as indicated in the abstract. Reuse of AIP content is subject to the terms at: http://jap.aip.org/about/rights_and_permissions